A NOTE ON FRACTAL STRUCTURE OF CUBIC GRAPHS IN THE MEAN-VARIANCE COORDINATES OF THE GRAPH'S RESOLVENT*

VLADIMIR EJOV†, SHMUEL FRIEDLAND‡, AND GIANG T. NGUYEN†.

Abstract. We consider the recently discovered [4] threadlike structure of the plot representing d-regular graphs in the mean-variance coordinates of exponential sums of the graph spectra. In this note we demonstrate that this fractal-like phenomenon is more ubiquitous by exhibiting it with the help of a different generating function, namely the mean and the variance of the graph adjacency matrix's resolvent. We also discuss the location of non-Hamiltonian graphs within this geometric structure.

Key words. Regular graph, spectrum, resolvent, fractal, Ihara-Selberg trace formula

AMS subject classifications. 05C45, 05C75, 11M36

1. Introduction. In [4], the following phenomenon was discovered. Let G be a connected cubic graph G of order n, and $\mathbf{A}$ be the adjacency matrix of G. The spectrum $\{\lambda_1, \ldots, \lambda_n\}$ of $\mathbf{A}$ of a cubic graph G is real and belongs to the segment $[-3, 3]$. The authors define the mean $\mu(\mathbf{A}, t)$ and variance $\sigma^2(\mathbf{A}, t)$ of the exponential sum of all eigenvalues of $t\mathbf{A}$ as follows:

$$\mu(\mathbf{A}, t) = \frac{1}{n} \sum_{i=1}^{n} \exp^{t\lambda_i}, \tag{1.1}$$

$$\sigma^2(\mathbf{A}, t) = \frac{1}{n} \sum_{i=1}^{n} \exp^{2t\lambda_i} - \mu^2(\mathbf{A}, t). \tag{1.2}$$

Note that for $t = 1$, the mean $\mu(\mathbf{A}, 1)$ is simply a scalar multiple of the Estrada index of the graph (see, for example, [5], [3] and [1]). Letting $t = \frac{1}{3}$, plot $(\mu(\mathbf{A}, \frac{1}{3}), \sigma^2(\mathbf{A}, \frac{1}{3}))$ across the set of all cubic graphs. The structures for $n = 14$ and 16 appear as follows:

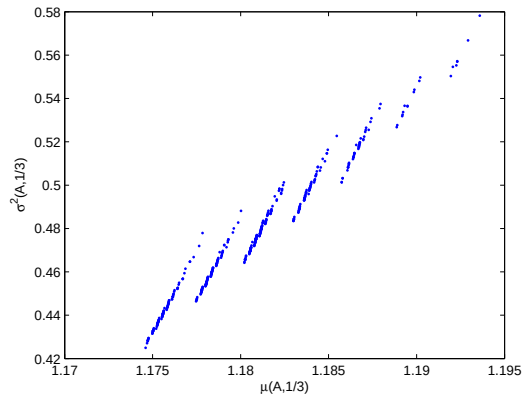

FIG. 1.1. *Mean-Variance plot for 14-vertex cubic graphs.*

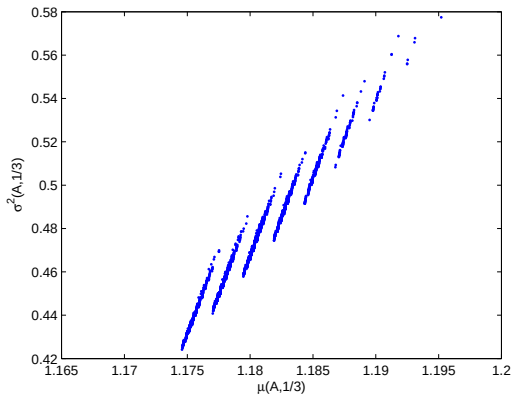

FIG. 1.2. *Mean-Variance plot for 16-vertex cubic graphs.*

From these plots, we can see that the mean-variance coordinates form thread-like clusters with similar slopes of and distances between consecutive clusters. Moreover, the variance $\sigma^2(\mathbf{A}, \frac{1}{3})$ at the bottom of each segment is strictly increasing from left to right of the plot. The authors of [4] coined the term *multifilars* to refer to these thread-like clusters, each of which is called a *filar*. They make an important observation that the overall structure is self-replicating or fractal-like. In particular, zooming in on each of these filars shows us similar but smaller sub-filars that are also made up of approximately straight

*The authors gratefully acknowledge the Australian Research Council (ARC) Discovery Grants No. DP0666632 and DP0984470, and the ARC Linkage International Grants No. LX0560049 and No. LX0881972.

†School of Mathematics of Statistics, University of South Australia. (Vladimir.Ejov@unisa.edu.au, Giang.Nguyen@unisa.edu.au.)

‡Department of Mathematics, Statistics, and Computer Science, University of Illinois at Chicago. (friedlan@uic.edu)

and parallel segments, shifted gradually from left to right. We illustrate this by showing plots of two successive enlargements of the first filar in Figure 1.1, in the following Figures 1.3 and 1.4:

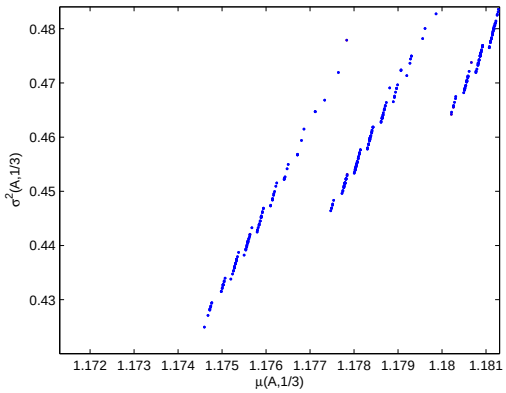

FIG. 1.3. *Zooming in, 1^{st} level.*

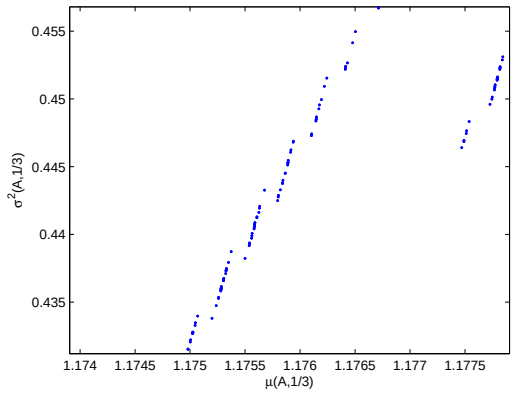

FIG. 1.4. *Zooming in, 2^{nd} level.*

Using Ihara-Selberg trace formula as in [6], the authors explain the filar memberships for each graph. In the overall clustering, all graphs belonging to each segment have the same number of triangles (cycles of length three) and these numbers strictly increase from the left most segment to the right most, starting from zero. In the first level of zooming-in, all graphs in a particular sub-segment have the same number of quadrangles (cycles of length four) while the number of triangles over all these sub-segments is fixed. This pattern repeats itself, with each higher level of zooming-in corresponding to a larger cycle size.

It is natural to query whether the exponential function is the only generating function that exhibits such a phenomenon. In this paper, we consider another frequently used matrix function in the spectral theory of linear operators (see, for example, [8]), that is, the resolvent of $t\mathbf{A}$ for $t \in (0, \frac{1}{3})$. It appears the phenomenon in [4] is reproduced in the mean-variance coordinates with different slopes of and distances between segments. We use a modification of the Ihara-Selberg trace formula [6] to justify the fractal structure of the observed plots and to give estimate for the slopes of and distances between segments, which are consistent with numerical evidence.

The further question: what other generating functions apart from the exponential sum of eigenvalues and the trace of the resolvent lead to a similar fractal structure of regular graphs, is beyond the scope of this paper and remains an interesting open question.

One of the famous graph theory problems is the *Hamiltonian cycle problem*, namely, given a graph, we have to determine whether there exists a simple cycle that goes through every vertex in the graph. Such a cycle is called a *Hamiltonian cycle*. If a graph possesses at least one Hamiltonian cycle, it is called a *Hamiltonian graph*, and a *non-Hamiltonian graph* otherwise. We observe that in the aforementioned self-replicating phenomenon, non-Hamiltonian graphs are separated in two groups. The first group contains *easy non-Hamiltonian* graphs that are located at the tops of (the most zoomed in) sub-filars. We call a non-Hamiltonian graph *easy* if it contains one or more *bridges*. This is because these bridges can be identified in polynomial time [9]. We call other non-Hamiltonian graphs *hard*. The second group contains *hard non-Hamiltonian* graphs that are found at the bottom ends of (the most zoomed in) sub-filars. In these sub-filars, the Hamiltonian graphs are strictly in between these two groups of non-Hamiltonian graphs.

2. Preliminaries. We briefly describe here a few definitions on *geodesics* that will be necessary for presenting the results. For an excellent introduction to graph theory and for more details on geodesics, the interested reader is referred to [2] and [6], respectively.

An *elementary homotopy* is a transformation of a closed walk of the following form:

$$(v_1, v_2, \ldots, v_i, \ldots, v_{k-1}, v_k, v_1) \mapsto (v_1, v_2, \ldots, v_i, v_j, v_i, \ldots, v_{k-1}, v_k, v_1),$$

where v_j is a neighbour of v_i, and the arrow can also be pointing in the opposite direction:

$$(v_1, v_2, \ldots, v_i, v_j, v_i, \ldots, v_{k-1}, v_k, v_1) \mapsto (v_1, v_2, \ldots, v_i, \ldots, v_{k-1}, v_k, v_1).$$

If one closed walk can be obtained from another by a sequence of elementary homotopies (in either direction of the arrow), they are said to be *homotopic*. A *homotopy class* is a set of closed walks such that every pair of closed walks in the set are homotopic. In a homotopy class of closed walks, the shortest walk is called a *closed geodesic*. In other words, *a closed geodesic* is a closed walk with no cycles of length 2, that is, $v_i \neq v_{i+2}$ for all i. As we are only concerned with closed geodesics in this paper, we will simply refer to them as *geodesics*.

Also known as a *short geodesic*, a *contractible* is a geodesic of length 0, or equivalently, a single vertex. A homotopy class of closed walks containing a geodesic of length 0 is equivalent to a homotopy class of closed walks such that each member is either a single vertex or a union of two or more joint cycles of length 2. A *long geodesic* is a geodesic of length > 0, which, from now on, we will simply refer to as a geodesic. A geodesic of length 3, 4 or 5 is equivalent to a cycle of length 3, 4 or 5. On the other hand, a geodesic of length 6 or longer can be a union of joint cycles. Consider a geodesic $g := (v_1, v_2, \ldots, v_l)$ of length l. Another geodesic is said to be a k-multiple of g, denoted as g^k, if it simply traces out g for k times: $g^k = (\{v_1, v_2, \ldots, v_l\}, \{v_1, v_2, \ldots, v_l\}, \ldots, \{v_1, v_2, \ldots, v_l\})$. A geodesic is said to be *primitive* if it is not a multiple of a shorter geodesic.

3. Formulae for first and second moments. Let us denote eigenvalues of the adjacency matrix $\mathbf{A}$ of a given cubic graph by λ_i, for $i = 1, \ldots, N$. We choose $t \in (0, \frac{1}{3})$ in order to guarantee that the inverse of $\mathbf{I} - t\mathbf{A}$ exists. For $i = 1, \ldots, N$, it is clear that eigenvalues of $(\mathbf{I} - t\mathbf{A})^{-1}$ are $(1 - t\lambda_i)^{-1}$. For each adjacency matrix $\mathbf{A}$, define the expected value function of $(1 - t\lambda_i)^{-1}$ to be

$$\mu(\mathbf{A}, t) := \frac{1}{N} \sum_{i=1}^{N} \frac{1}{1 - t\lambda_i} = \frac{1}{N} \mathrm{Tr}[(\mathbf{I} - t\mathbf{A})^{-1}], \tag{3.1}$$

and the variance function to be

$$\begin{aligned} \sigma^2(\mathbf{A}, t) &:= \frac{1}{N} \mathrm{Tr}[(\mathbf{I} - t\mathbf{A})^{-2}] - \mu^2(\mathbf{A}, t) \\ &= \frac{1}{N} \sum_{i=1}^{N} \frac{1}{(1 - t\lambda_i)^2} - \mu^2(\mathbf{A}, t). \end{aligned} \tag{3.2}$$

For our experiments, we choose $t = \frac{1}{9} \in (0, \frac{1}{3})$. Figure 3.1 shows the plot of $(\mu(\mathbf{A}), \sigma^2(\mathbf{A}))$ across all 509 cubic graphs of size 14, which exhibits a fractal-like structure.

In order to explain why pairs of coordinates of certain graphs belong to particular filars, we start by establishing alternative formulae for $\mu(\mathbf{A}, t)$ and $\sigma^2(\mathbf{A}, t)$. Let p_ℓ be the number of all walks of length ℓ in the graph G, for $\ell \geq 0$. It is well known (see, for example, [10]) that $[\mathbf{A}^\ell]_{ii}$ is the number of closed walks of length ℓ starting at i. Hence,

$$\begin{aligned} \mu(\mathbf{A}, t) &= \frac{1}{N} \mathrm{Tr}\left[(\mathbf{I} - t\mathbf{A})^{-1}\right] = \frac{1}{N} \mathrm{Tr}\left[\mathbf{I} + t\mathbf{A} + t^2\mathbf{A}^2 + \cdots\right] \\ &= \frac{1}{N}\left[n + tp_1 + t^2p_2 + t^3p_3 + \cdots\right] = \frac{1}{N} \sum_{i=0}^{\infty} t^i p_i. \end{aligned} \tag{3.3}$$

The infinite sum in (3.3) resembles the trace of the matrix exponential of $t\mathbf{A}$:

$$\mathrm{Tr}[\exp^{t\mathbf{A}}] = \sum_{i=0}^{\infty} \frac{t^i}{i!} p_i.$$

Recall that a geodesic is the shortest walk of its homotopy class, and a geodesic is a short geodesic if it has length 0 and a long geodesic otherwise. Let $C_1(t)$ and $C_2(t)$ be the contributions to (3.3) from homotopy classes of short geodesics and long geodesics, respectively. Then,

$$\mu(\mathbf{A}, t) = \frac{1}{N}\left(C_1(t) + C_2(t)\right). \tag{3.4}$$

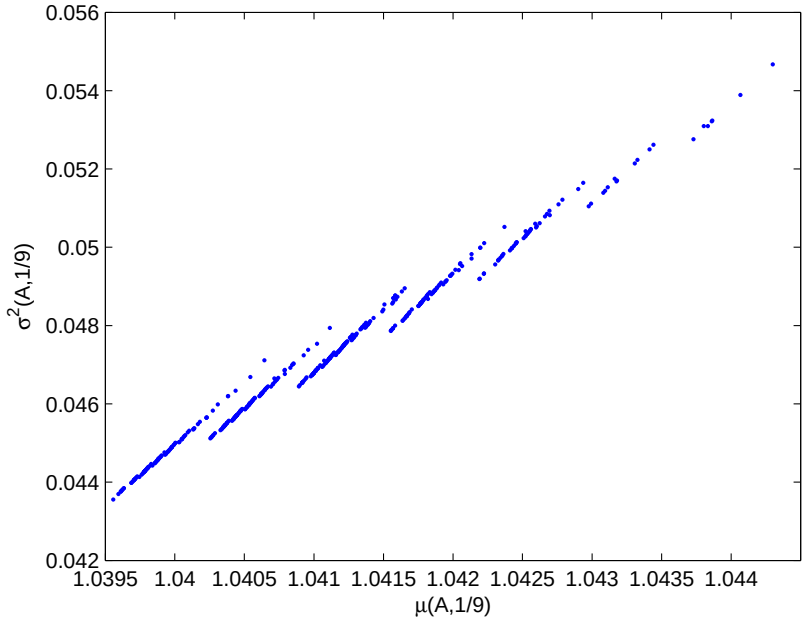

FIG. 3.1. *Mean-Variance (trace of resolvent) plot for 14-vertex cubic graphs.*

By equations (19) and (20) in [6],

$$C_1(t) = N\frac{3\sqrt{1-8t^2}-1}{2(1-9t^2)}. \tag{3.5}$$

By equations (26) and (27) in [6],

$$C_2(t) = \sum_{\gamma\in G}\frac{\Lambda(\gamma)}{\sqrt{1-8t^2}}\left(\frac{1-\sqrt{1-8t^2}}{4t}\right)^{|\gamma|}, \tag{3.6}$$

where γ is a long geodesic in G, $|\gamma|$ is its length and $\Lambda(\gamma) = |\gamma'|$ if γ is a multiple of a primitive geodesic γ'. If γ is primitive itself, then $\Lambda(\gamma) = |\gamma|$.

Define $\Theta(t) := \dfrac{1-\sqrt{1-8t^2}}{4t}$. Substituting (3.5) and (3.6) into (3.4), we have

$$\mu(\mathbf{A},t) = \frac{3\sqrt{1-8t^2}-1}{2(1-9t^2)} + \frac{1}{N}\sum_{\gamma\in G}\frac{\Lambda(\gamma)}{\sqrt{1-8t^2}}\Theta^{|\gamma|}(t). \tag{3.7}$$

Recall that a geodesic is said to be a k-multiple of g, denoted as g^k, if it k times traces out g: $g^k = (\{v_1,v_2,\ldots,v_l\},\{v_1,v_2,\ldots,v_l\},\ldots,\{v_1,v_2,\ldots,v_l\})$. Consequently, if we consider some geodesic γ that is a k-multiple of a primitive geodesic γ', then $|\gamma| = k|\gamma'|$. The set of all long geodesics in a graph G can be partitioned into sets of primitive geodesics and their k-multiples, for $k = 1,\ldots,N$. Therefore, by denoting primitive long geodesics by ζ, we transform equation (3.7) to:

$$\begin{aligned}\mu(\mathbf{A},t) &= \frac{3\sqrt{1-8t^2}-1}{2(1-9t^2)} + \frac{1}{N}\sum_{\zeta\in G}\sum_{k=1}^{\infty}\frac{|\zeta|}{\sqrt{1-8t^2}}\Theta^{k|\zeta|}(t)\\ &= \frac{3\sqrt{1-8t^2}-1}{2(1-9t^2)} + \frac{1}{N}\sum_{\zeta\in G}\frac{|\zeta|}{\sqrt{1-8t^2}}\sum_{k=1}^{\infty}\Theta^{k|\zeta|}(t).\end{aligned}$$

As $t \in \left(0, \frac{1}{3}\right), \Theta(t) \in (0,1)$. Hence,

$$\begin{aligned}\mu(\mathbf{A},t) &= \frac{3\sqrt{1-8t^2}-1}{2(1-9t^2)} + \frac{1}{N}\sum_{\zeta\in G}\frac{|\zeta|}{\sqrt{1-8t^2}}\left[\frac{\Theta^{|\zeta|}(t)}{1-\Theta^{|\zeta|}(t)}\right] \\ &= \frac{3\sqrt{1-8t^2}-1}{2(1-9t^2)} + \frac{1}{N}\sum_{\zeta\in G}\frac{|\zeta|}{\sqrt{1-8t^2}}\left[\frac{(1-\sqrt{1-8t^2})^{|\zeta|}}{(4t)^{|\zeta|}-(1-\sqrt{1-8t^2})^{|\zeta|}}\right]. \end{aligned} \tag{3.8}$$

Let ℓ be the length of a primitive long geodesic, $\ell \geq 3$ and $\{m_3, m_4, m_5, \ldots\}$ be the *length spectrum* of the graph where m_ℓ is the number of *non-oriented* primitive long geodesics of length ℓ. We can rewrite (3.8) as

$$\begin{aligned}\mu(\mathbf{A},t) &= \frac{3\sqrt{1-8t^2}-1}{2(1-9t^2)} + \frac{2}{N}\sum_{\ell=3}^{\infty}\frac{\ell m_\ell}{\sqrt{1-8t^2}}\left[\frac{(1-\sqrt{1-8t^2})^{\ell}}{(4t)^{\ell}-(1-\sqrt{1-8t^2})^{\ell}}\right] \\ &= H(t) + \frac{2}{N}\sum_{\ell=3}^{\infty} m_\ell F_\ell(t), \end{aligned} \tag{3.9}$$

where

$$H(t) = \frac{3\sqrt{1-8t^2}-1}{2(1-9t^2)}, \tag{3.10}$$

and

$$F_\ell(t) = \frac{\ell}{\sqrt{1-8t^2}}\left[\frac{(1-\sqrt{1-8t^2})^{\ell}}{(4t)^{\ell}-(1-\sqrt{1-8t^2})^{\ell}}\right]. \tag{3.11}$$

By equation (3.2),

$$\begin{aligned}\sigma^2(\mathbf{A},t) &= \frac{1}{N}\mathrm{Tr}[(\mathbf{I}-t\mathbf{A})^{-1}(\mathbf{I}-t\mathbf{A})^{-1}] - \mu^2(\mathbf{A},t) \\ &= \frac{1}{N}\mathrm{Tr}[\mathbf{I} + 2t\mathbf{A} + 3t^2\mathbf{A}^2 + 4t^3\mathbf{A}^3 + \cdots] - \mu^2(\mathbf{A},t) \\ &= \frac{1}{N}\mathrm{Tr}\left(\frac{d}{dt}[t\mathbf{I} + t^2\mathbf{A} + t^3\mathbf{A}^2 + t^4\mathbf{A}^3 + \cdots]\right) - \mu^2(\mathbf{A},t) \\ &= \frac{1}{N}\frac{d}{dt}\left(t\mathrm{Tr}[(\mathbf{I}-t\mathbf{A})^{-1}]\right) - \mu^2(\mathbf{A},t) \\ &= \mu(\mathbf{A},t) + t\frac{d}{dt}\mu(\mathbf{A},t) - \mu^2(\mathbf{A},t). \end{aligned} \tag{3.12}$$

By equations (3.9) and (3.12), we have

$$\begin{aligned}\sigma^2(\mathbf{A},t) &= H(t) + \frac{2}{N}\sum_{\ell=3}^{\infty} m_\ell F_\ell(t) + t\frac{d}{dt}\left[H(t) + \frac{2}{N}\sum_{\ell=3}^{\infty} m_\ell F_\ell(t)\right] \\ &\quad -H^2(t) - \left[\frac{2}{N}\sum_{\ell=3}^{\infty} m_\ell F_\ell(t)\right]^2 - \frac{4}{N}\sum_{\ell=3}^{\infty} m_\ell H(t) F_\ell(t) \\ &= H(t) + tH'(t) - H^2(t) + \frac{2}{N}\sum_{\ell=3}^{\infty} m_\ell F_\ell(t) + t\left(\frac{2}{N}\sum_{\ell=3}^{\infty} m_\ell F_\ell'(t)\right) \\ &\quad -\frac{4}{N^2}\left[\sum_{\ell=3}^{\infty} m_\ell F_\ell(t)\right]^2 - \frac{4}{N}H(t)\sum_{\ell=3}^{\infty} m_\ell F_\ell(t), \end{aligned} \tag{3.13}$$

where

$$H'(t) = -3\,\frac{t\left(-5+36\,t^2+3\,\sqrt{1-8\,t^2}\right)}{\sqrt{1-8\,t^2}\left(-1+9\,t^2\right)^2},$$

and

$$F'_\ell(t) =$$

$$\frac{\ell(1-\sqrt{1-8t^2})^\ell(8(4t)^\ell t^2-8(1-\sqrt{1-8t^2})^\ell t^2-8(4t)^\ell t^2\sqrt{1-8t^2}+8\ell(4t)^\ell t^2+8(1-\sqrt{1-8t^2})^\ell\sqrt{1-8t^2}-(4t)^\ell\ell+\ell\sqrt{1-8t^2}(4t)^\ell)}{t(-1+\sqrt{1-8t^2})\sqrt{1-8t^2}(-1+8t^2)(-(4t)^\ell+(1-\sqrt{1-8t^2})^\ell)^2)}.$$

In particular, for $t = \frac{1}{9}$, equations (3.9) and (3.13) simplify to, respectively,

$$\mu(\mathbf{A},\tfrac{1}{9}) \approx 1.0395 + \frac{2}{N}\sum_{\ell=3}^{\infty} m_\ell F_\ell\left(\tfrac{1}{9}\right), \text{ and} \tag{3.14}$$

$$\sigma^2(\mathbf{A},\tfrac{1}{9}) \approx 0.0433 + \frac{2}{N}\sum_{\ell=3}^{\infty} m_\ell F_\ell(\tfrac{1}{9}) + \frac{1}{9}\left(\frac{2}{N}\sum_{\ell=3}^{\infty} m_\ell \left[F'_\ell(t)\right]_{t=\frac{1}{9}}\right)$$
$$-\frac{4}{N^2}\left[\sum_{\ell=3}^{\infty} m_\ell F_\ell\left(\tfrac{1}{9}\right)\right]^2 - \frac{4.1580}{N}\sum_{\ell=3}^{\infty} m_\ell F_\ell\left(\tfrac{1}{9}\right), \tag{3.15}$$

where

$$F_\ell\left(\tfrac{1}{9}\right) = \frac{9}{73}\,\frac{\ell\sqrt{73}\left(1-\frac{1}{9}\sqrt{73}\right)^\ell}{\left(\frac{4}{9}\right)^\ell - \left(1-\frac{1}{9}\sqrt{73}\right)^\ell},$$

and

$$\left[F'_\ell(t)\right]_{t=\frac{1}{9}} = \frac{81}{5329}\,\frac{\ell\left(9-\sqrt{73}\right)^\ell\left(-72(4)^\ell\sqrt{73}+584(4)^\ell+72\sqrt{73}\left(9-\sqrt{73}\right)^\ell-584\left(9-\sqrt{73}\right)^\ell-5913\,4^\ell\ell+657\sqrt{73}\ell 4^\ell\right)}{\left(-9+\sqrt{73}\right)\left(-4^\ell+\left(9-\sqrt{73}\right)^\ell\right)^2}.$$

4. Rates of change and dominant terms. Note that the following analysis of the rates of change, dominant terms, slopes of and distances between filars is similar to arguments presented in [4], in which the fractal-like multifilar phenomenon was first discovered.

For various fixed values of $t \in (0, \frac{1}{3})$, our experiments show that both function $F_\ell(t)$ and its partial derivative $F'_\ell(t)$ are rapidly decreasing as ℓ grows. In fact, we observe that $F_\ell\left(\frac{1}{9}\right) \le C_1 10^{-\ell}$ and $\left[F'_\ell(t)\right]_{t=\frac{1}{9}} \le C_2 10^{-\ell}$ for some positive constants C_1 and C_2. It is reasonable to assume that on the other hand, m_ℓ does not grow as fast as $C10^\ell$ for some positive constant C as ℓ increases.

As a result, the contribution of the quadratic terms of $F_\ell\left(\frac{1}{9}\right)$ in (3.15) is insignificant and $\ell = 3$ is the dominant term in the infinite sums in (3.14) and (3.15). Recall our observation that each filar, where each graph has m_3 triangles, is made up of sub-filars. Each of these sub-flars consists of graphs that have exactly m_4 rectangles, with $m_4 = 0$ for the left-most sub-filar and m_4 increases by 1 from one sub-filar to the next sub-filar to the right. Consequently, the lower endpoint of each filar is most likely to contain a graph that has m_3 triangles and zero rectangles. Therefore, from (3.14) and (3.15), with $t = \frac{1}{9}$, we can approximate the coordinates for the lower end point of each filar with graphs possessing m_3 triangles by:

$$\mu(m_3) = 1.0395 + \frac{2}{N} m_3 F_3\left(\tfrac{1}{9}\right), \text{ and} \tag{4.1}$$

$$\sigma^2(m_3) = 0.0433 + \frac{2}{N} m_3 F_3(\tfrac{1}{9}) + \frac{1}{9}\left(\frac{2}{N} m_3 \left[F'_3(t)\right]_{t=\frac{1}{9}}\right)$$
$$-\frac{4.1580}{N} m_3 F_3\left(\tfrac{1}{9}\right). \tag{4.2}$$

Consequently, let $k \in [0, \infty)$, then the line (see Figure 4.1) that goes through the lower end points of filars can be approximated by the parametric line $(x(k), y(k))$, where

$$x(k) = 1.0395 + kF_3(\tfrac{1}{9}) \approx 1.0395 + 0.0047k, \tag{4.3}$$

$$y(k) = 0.0433 + k\left(F_3(t) + \frac{1}{9}\left[F'_3(t)\right]_{t=\frac{1}{9}} - 2.0790F_3\left(\tfrac{1}{9}\right)\right) \approx 0.0433 + 0.0103k. \tag{4.4}$$

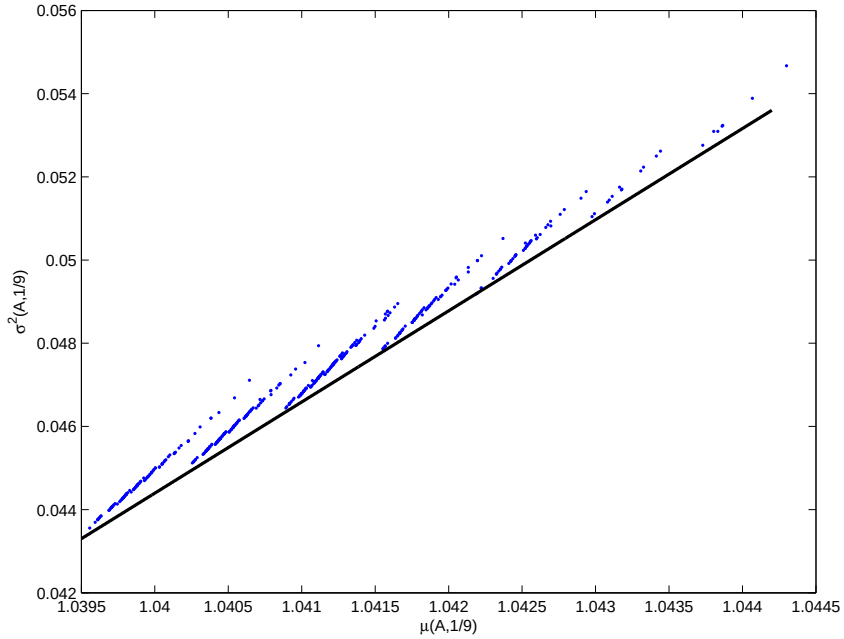

FIG. 4.1. *Mean-Variance (trace of resolvent) plot for 14-vertex cubic graphs*

The slope of the line parametrically described by (4.3) and (4.4) (and represented by the black line in Figure 4.1) is $0.0103/0.0047 = 2.1901$, which is close to the experimental value of 2.04 for cubic graphs of 14 vertices.

The observation that $\ell = 3$ is is the dominant term in the infinite sums in (3.14) and (3.15) also explains why in the fractal-like structure in Figure 3.1 if two cubic graphs have the same number of triangles, then they belong to the same filar. Similarly, we can explain the membership of sub-filars of various levels. Each filar, where all graphs have m_3 triangles, can be approximated (see Figure 4.2) by a line parametrically defined as follows:

$$\begin{aligned} x(s) &= 1.0395 + \frac{2}{N} m_3 F_3\left(\tfrac{1}{9}\right) + s F_4\left(\tfrac{1}{9}\right) \\ &= 1.0395 + \frac{2}{N} 0.0047 m_3 + 0.0007 s, \qquad (4.5) \\ y(s) &= 0.0433 + \frac{2}{N} m_3 \left(F_3(\tfrac{1}{9}) + \frac{1}{9}\left[F_3'(t)\right]_{t=\frac{1}{9}} - 2.0790 F_3\left(\tfrac{1}{9}\right) \right) \\ &\quad + s \left(F_4(\tfrac{1}{9}) + \frac{1}{9}\left[F_4'(t)\right]_{t=\frac{1}{9}} - 2.0790 F_4\left(\tfrac{1}{9}\right) \right) \\ &= 0.0433 + \frac{2}{N} 0.0103 m_3 + 0.0023 s. \qquad (4.6) \end{aligned}$$

The slope of each filar is approximately:

$$\frac{F_4(\frac{1}{9}) + \frac{1}{9}\left[F_4'(t)\right]_{t=\frac{1}{9}} - 2.0790 F_4\left(\frac{1}{9}\right)}{F_4\left(\frac{1}{9}\right)} \approx 3.2448,$$

which is independent of the graph size N. Consider two consecutive filars, consisting of graphs containing exactly $m_3^{(1)}$ and $m_3^{(2)}$ triangles respectively. Then the line approximating the first filar is parametrically

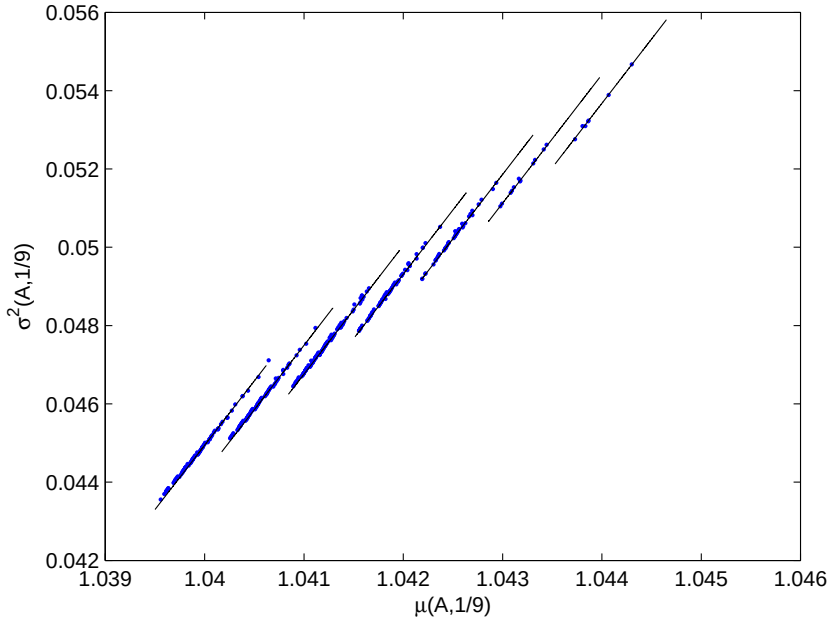

FIG. 4.2. *Mean-Variance (trace of resolvent) plot for 14-vertex cubic graphs.*

defined by:

$$\bar{x}(s_1) = 1.0395 + \frac{2}{N}0.0047m_3^{(1)} + 0.0007s_1,$$
$$\bar{y}(s_1) = 0.0433 + \frac{2}{N}0.0103m_3^{(1)} + 0.0023s_1,$$

and the line approximating the second filar is parametrically defined by:

$$\hat{x}(s_2) = 1.0395 + \frac{2}{N}0.0047m_3^{(2)} + 0.0007s_2,$$
$$\hat{y}(s_2) = 0.0433 + \frac{2}{N}0.0103m_3^{(2)} + 0.0023s_2,$$

In order to find out the horizontal distance between two filars approximated by the parametric lines $(\bar{x}(s_1), \bar{y}(s_2))$ and $(\hat{x}(s_1), \hat{y}(s_2))$, firstly, we need to find out s_1 and s_2 such that $\bar{y}(s_1) = \hat{y}(s_2)$:

$$0.0433 + \frac{2}{N}0.0103m_3^{(1)} + 0.0023s_1 = 0.0433 + \frac{2}{N}0.0103m_3^{(2)} + 0.0023s_2$$
$$s_1 = s_2 + 0.0206\frac{m_3^{(2)} - m_3^{(1)}}{N}.$$

Then the horizontal distance between the two aforementioned filars is:

$$\hat{x}(s_2) - \bar{x}\left(s_2 + 0.0206\frac{m_3^{(2)} - m_3^{(1)}}{N}\right)$$
$$= \frac{2}{N}0.0047m_3^{(2)} + 0.0007s_2 - \frac{2}{N}0.0047m_3^{(1)} - 0.0007\left(s_2 + 0.0206\frac{m_3^{(2)} - m_3^{(1)}}{N}\right)$$
$$= 0.0094\frac{m_3^{(2)} - m_3^{(1)}}{N}.$$

Hence, the horizontal distance between two consecutive filars decreases as the graph size N increases, so the filars are closer to each other as the graphs get larger.

5. Self-replicating Structure and Hamiltonicity. Due to the interest in the Hamiltonian cycle problem, we reconstruct the variance-versus-mean plot in Figure 3.1, but distinguish between Hamiltonian and non-Hamiltonian graphs. Each pair of coordinates $(\mu_{\mathbf{A}}(\frac{1}{9}), \sigma^2_{\mathbf{A}}(\frac{1}{9}))$ of a 14-vertex cubic graph is a dot on this reconstructed plot (see Figure 5.1) if the graph is Hamiltonian, and a cross if the graph is non-Hamiltonian.

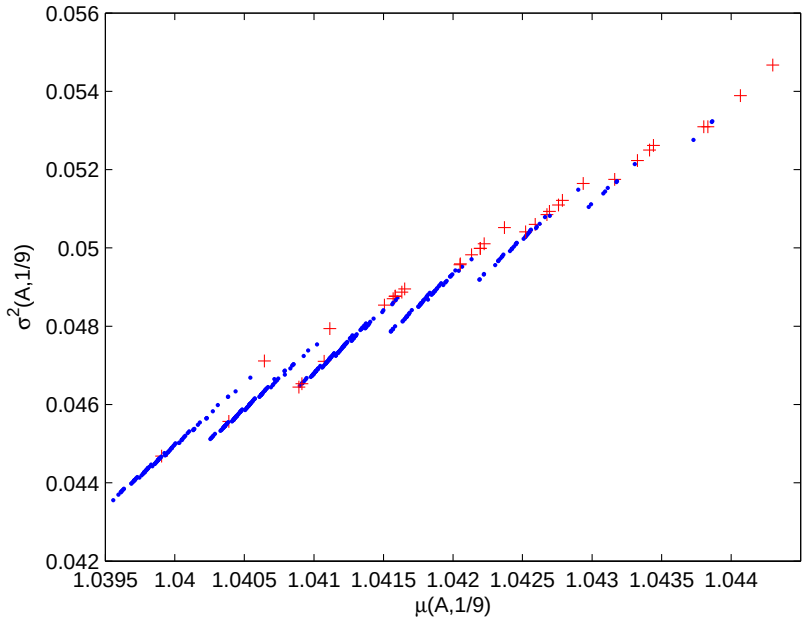

FIG. 5.1. *Mean-Variance plot for 14-vertex cubic graphs and Hamiltonicity.*

Two graphs are *cospectral* if they share the same spectrum, and are *non-cospectral* otherwise. There are no cospectral cubic graphs with fewer than 14 vertices, and there are at least three pairs of cospectral cubic graphs on 14 vertices [7]. Therefore, there are three pairs of graphs of which the coordinates in the above plot are the same. However, as these three pairs are all Hamiltonian graphs, their cospectral property does not affect our observation on the fractal-like multifilar structure and Hamiltonicity.

Glancing at the plot in Figure 5.1, it is easy to think that while the majority of non-Hamiltonian graphs are located in the top and bottom parts of filars, some of them are mixed amongst dots representing Hamiltonian graphs. However, if we zoom in on the innermost[1] sub-filars, we will find that all non-Hamiltonian graphs are strictly at the top and the bottom of these sub-filars, and there is no mixing between Hamiltonian and non-Hamiltonian graphs. While it is not practical to show all plots which zoom in on the innermost sub-filars, we present here one of these zooming-in plots (see Figure 5.2) to illustrate our observation. All crosses that can be seen clearly in this plot are either at the top or the bottom of their sub-filars.

We have not yet been able to explain why the absence of Hamiltonian cycles make non-Hamiltonian graphs gather around the top and the bottom of their innermost sub-filars. However, we have experimentally found the answer as to which non-Hamiltonian graphs are at the higher end while the rest are at the lower.

Briefly, non-Hamiltonian graphs that are located at the top of their sub-filars are *bridge graphs*. A bridge graph is a graph that contains at least one *bridge*, that is, an edge the removal of which disconnects the graph. Section 57 in [9] contains a very natural theorem which states that all bridge graphs are

[1] When we can no longer zoom in on a filar to obtain a similar structure made up of smaller filars, we are at the innermost sub-filars.

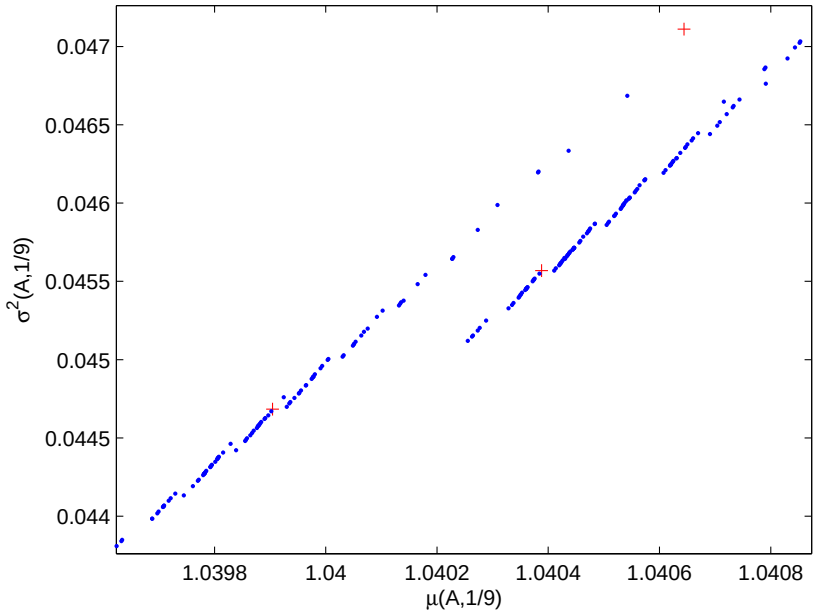

FIG. 5.2. *Mean-Variance plot - zooming in.*

non-Hamiltonian. These graphs can be identified in polynomial time; hence, we refer to them as *easy non-Hamiltonian graphs*. A non-Hamiltonian graph that is not an easy non-Hamiltonian graph is a *hard non-Hamiltonian graph*. The latter group are found to be at the bottom of their sub-filars. These hard non-Hamiltonian graphs constitute the underlying difficulty of the NP-hard complexity to the Hamiltonian cycle problem. For example, Figure 5.3 shows the plot of coordinates $(\mu_{\mathbf{A}}(\frac{1}{9}), \sigma^2_{\mathbf{A}}(\frac{1}{9}))$ for 10-vertex (connected) cubic graphs, of which there are 19, including 17 Hamiltonian ones.

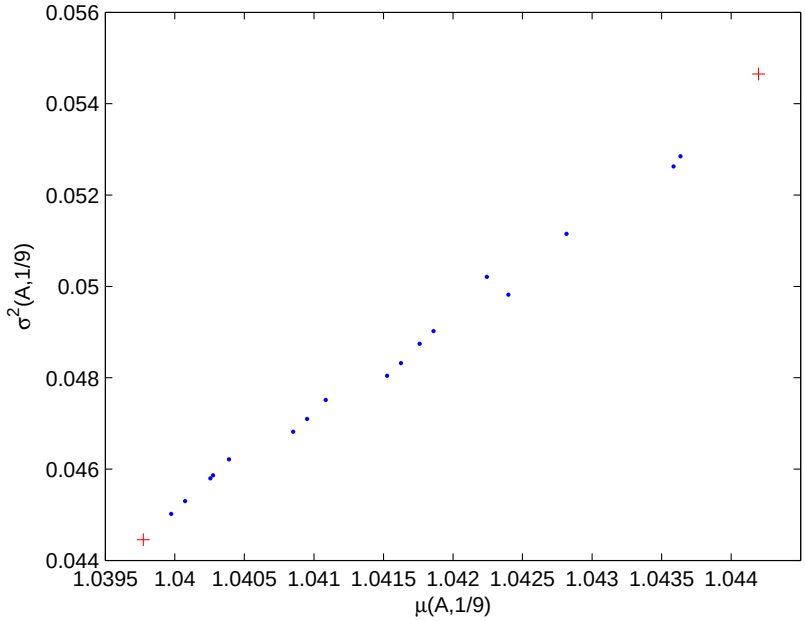

FIG. 5.3. *Mean-Variance plot for 10-vertex cubic graphs and Hamiltonicity.*

One non-Hamiltonian graph is a bridge graph (see Figure 5.4), represented by the cross at the top right

of the plot. The other non-Hamiltonian graph is the well-known Petersen graph (see Figure 5.5), which is not a bridge graph and is represented by the cross at the bottom left of the same plot.

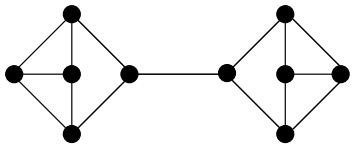

FIG. 5.4. *The only cubic bridge graph of size 10.*

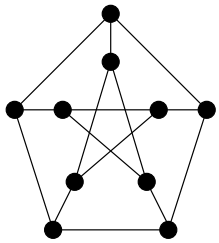

FIG. 5.5. *Petersen graph.*

It would be interesting to obtain a theoretical justification of this observation.

6. Acknowledgements. The authors would like to thank J. A. Filar and P. Zograf for numerous useful discussions.

REFERENCES

[1] J. A. de la Peña, I. Gutman, and R. Rada. Estimating the Estrada index. *Linear Algebra Appl.* 427 (2007), 70–76.
[2] F. Harary. *Graph Theory.* (1969), Addison-Wesley, Reading, MA.
[3] I. Gutman and Ante Graovac. Estrada index of cycles and paths. *Chem. Phys. Lett.* 436 (2007), 294–296.
[4] V. Ejov, J. A. Filar, S. K. Lucas and P. Zograf. Clustering of spectra and fractals of regular graphs. *J. Math. Anal. Appl.* 333 (2007), 236-246.
[5] E. Estrada. Characterization of 3D molecular structure. *Chem. Phys. Lett.* 319 (2000), 713-718.
[6] P. Mnev. Discrete path integral approach to the Selberg trace formula for regular graphs. *Comm. Math. Phys.* 274 (2006), 233–241.
[7] J. A. Filar, A. Gupta and S. K. Lucas. Connected co-spectral graphs are not necessarily both Hamiltonian. *Aust. Math. Soc. Gaz.* 32:3 (2005), 193.
[8] V. Müller. *Spectral Theory of Linear Operators and Spectral Systems in Banach Algebras.* Series: Operator Theory: Advances and Applications, 139 (2007), Birkhäuser.
[9] A. Sainte-Lague. Les reseaux (ou graphes). *Memorial des sciences math.* 18 (1926).
[10] E. van Dam and W. Haemers. Which graphs are determined by their spectrum? *Linear Algebra Appl.* 373 (2003), 241–272.